

# Stochastic Geometry-Based Interference Characterization for RF and VLC-Based Vehicular Communication System

Gurinder Singh , Anand Srivastava, and Vivek Ashok Bohara , *Senior Member, IEEE*

**Abstract**—In this article, we characterize various aspects of stochastic behavior of intervehicular interference by modeling location of road vehicles as a spatial Poisson point process. We make use of various analytical tools of stochastic geometry to provide an analytical framework to access the performance for both vehicular-radio frequency (V-RF) communication and vehicular-visible light communication (V-VLC) for dense, medium, and sparse traffic scenarios. The developed framework is also precise in terms of capturing the impact of reducing field-of-view (FOV) of receiver on the level of interference experienced from interferers for V-VLC. The performance has been evaluated and compared under normal atmospheric conditions as well as different environmental deterrents viz., light fog, dense fog, and dry snow conditions in terms of probability of successful transmission as a performance metric. Irrespective of any traffic scenario, the performance of V-VLC communication under normal atmospheric condition always outperforms V-RF communication. However, the performance of V-RF communication is comparatively better than V-VLC under various environmental deterrents. The proposed result motivates the benefit of employing RF-based or VLC-based vehicular-to-vehicular (V2V) communication which takes into account different environmental conditions as well as meets the diverse application requirements for future intelligent transportation system.

**Index Terms**—Correction function, critical radius, illumination intensity (power) pattern, stochastic geometry, visible light communications (VLC).

## I. INTRODUCTION

VEHICLE-TO-VEHICLE (V2V) communication based on dedicated short range communication (DSRC) at 5.9 GHz [1] shows promising potential that can meet diverse requirement of future intelligent transport system (ITS) with enhanced passenger safety, reduced traffic accidents, and congestion. Currently, ITS research activities, standardization, and products mainly rely on deployment of vehicular-radio frequency (V-RF)-based technologies with wireless access for vehicular networks. The conventional V-RF communication experiences unwanted packet loss, longer delays, and lower packet reception rate (PRR)

especially during peak hours when traffic congestion is quite high [2]. In addition to the above, RF-based transceiver design is complex with relatively more added cost to the vehicle's price in form of on-board unit (OBU) installation. In recent years, the vehicular-visible light communication (V-VLC)-based technology has gained considerable attention among researchers. V-VLC offer advantages such as lower costs, higher PRR, less delays, and complexity by utilizing the existing vehicle's headlamp and taillight for exchange of information, thus satisfying illumination as well as communication requirements. However, conventional V-RF has superior communication range and wider coverage area as compared to V-VLC [3]. It should be noted here that both V-RF and V-VLC are complementary to each other. For instance, V-RF-based technology may be appropriate for long range communication, whereas V-VLC-based technology may be suitable for high traffic density scenarios.

V-RF communication in the 5.9-GHz frequency band has virtually no atmospheric or weather effects;<sup>1</sup> the main contributors are thermal noise at the antenna receiver and the interference caused from other simultaneous transmissions [4]. Unlike V-RF communication, the performance of V-VLC is considerably affected under various environmental deterrents such as rain, light fog, dense fog, dry snow, wet snow, etc. [5].

### A. Literature Review

The ITS [6] aims to integrate the existing state-of-the-art cooperative technologies with the purpose of enhancing road safety and efficiency of the transportation system. This will also lead to reduced traffic congestion as well as minimize the carbon footprints. Several technologies were proposed and investigated for communications between vehicles and roadside infrastructures, for instance, infrared [7], bluetooth [8], 3G [9], [10] LTE [11], or even hybrid of these aforementioned technologies [12]. The primary focus has always been on the V-RF communication which is regulated by the IEEE 802.11p standards. Currently, the impact of vehicle-to-everything (V2X) communications on the amount of RF spectrum usages is quite low, but it is expected to significantly increase in the near future. Such small RF bands can quickly suffer from interference when large number of vehicles located in the same vicinity try to communicate simultaneously. There are a number of solutions to

Manuscript received December 12, 2019; revised April 14, 2020, July 5, 2020, and September 4, 2020; accepted September 6, 2020. This work was supported by the Visvesvaraya Ph.D. Scheme by Ministry of Electronics and Information Technology, Government of India, implemented by Digital India Corporation. (Corresponding author: Gurinder Singh.)

The authors are with the Department of Electronics and Communication Engineering, Indraprastha Institute of Information Technology, New Delhi 110020, India (e-mail: gurinders@iiitd.ac.in; anand@iiitd.ac.in; vivek.b@iiitd.ac.in).

Digital Object Identifier 10.1109/JSYST.2020.3027883

<sup>1</sup>Recommendation ITU-R P.525-2, 1994

address this potential bandwidth congestion problem. One such possible solution is the usage of VLC in context to vehicular scenario.

In [13]–[15], the authors have shown the feasibility of VLC-based model for V2V communications using vehicle's LED headlamp and photodiodes. The critical issue for vehicular VLC channels is the weather conditions which has received insufficient attention in literature so far. In [5], the authors document the effects of fog and rain on the performance of V-VLC. In [16] and [17], Kim *et al.* employed a laboratory chamber and experimentally evaluated the effect of artificially generated rain and fog on the received optical signal for a red LED (that can be potentially used as a taillight). In [18] and [19], the authors characterize the daylight beam pattern of empirically measured low and high beams of LED headlights. Apart from the impact of various environmental deterrents, interference from neighboring vehicles is also a major source of degradation for V-VLC channel. Interference can be modeled as noise which is independent from the desired signal of interest and Gaussian distributed. Most of these comprehensive studies have not considered the impact of interference from multiple interferers as well as various environmental deterrents on performance of V-VLC based on illumination intensity (power) pattern for a typical vehicle headlamp module.

In mathematics, stochastic geometry is the study of random spatial patterns. It allows one to study the average behavior over many spatial realizations for a network whose nodes are assumed to be placed according to some probability distribution [20], [21]. Stochastic geometry can be used to characterize the randomness in the spatial distribution of vehicles [22]. Most of the existing literature has used stochastic geometry tools to evaluate the performance of wireless networks wherein location of base stations and users are spatially distributed by Poisson point process (PPP). The work presented in [23] and [24] have characterized the interference in context to cellular network based on stochastic analysis. The application of stochastic geometry in context to vehicular ad hoc networks (VANET) has been to evaluate the successful transmission rate by modeling spatial distribution of road vehicles according to single-dimensional PPP as presented in [25] and [26]. In order to capture the effect of medium access (MAC) control to determine probability of successful transmission, the authors in [27] have used Matérn hardcore process for modeling PPP vehicle distribution.

To the best of our knowledge, the work presented in this article is the first to compare and model the statistical behavior of interference experienced by conventional V-RF and V-VLC by utilizing various analytical tools of stochastic geometry. The performance of conventional V-RF and V-VLC communication under various environmental deterrents such as light fog, dense fog, and dry snow condition has been evaluated in terms of probability of successful transmission as performance metric. Further, the impact of interference from multiple interferers on performance of V-VLC based on illumination intensity (power) pattern for a typical vehicle headlamp has also been demonstrated for various environmental conditions.

## B. Contribution

The key contribution of the proposed work can be summarized as follows.

- 1) This article gives an analytic framework for estimating the average signal-to-interference-plus-noise ratio (SINR) and thus provides the expected performance for both conventional V-RF as well as V-VLC using various analytical tools of stochastic geometry. The developed framework is also precise in terms of capturing the impact of field-of-view (FOV) of the photo-detector (PD) receiver on the number of interferers and distribution of the aggregate interference for a V-VLC communication system.
- 2) The impact of mean interference as well as various environmental deterrents viz., light fog, dense fog, and dry snow conditions on received illumination power (intensity) pattern for original equipment manufacturer (OEM) LED headlamp has also been demonstrated.
- 3) The performance of conventional RF-based V2V and VLC-based V2V under the above environmental deterrents has been evaluated and compared in terms of probability of successful transmission as a performance metric.

This article has been structured as follows. Section II presents system model and gives analytical framework to characterize the level of interference experienced by conventional V-RF communication as well as V-VLC using various analytic tools of stochastic geometry. The expression for probability of successful transmission has been derived in Section III. The performance of both the technologies have been evaluated in terms of performance metric as described before with useful insights in Section IV. Finally, concluding remarks are given in Section V.

*Notation:*  $\xi_c(\cdot)$  and  $\xi(\cdot)$  defines complementary error function and error function, respectively,  $\mathbb{P}[\cdot]$  denotes probability of an event,  $\mathbb{E}_Y[\cdot]$  is the expectation of its argument over random variable (RV)  $Y$  and  $\Im$  denotes imaginary part of complex number.  $\mathbb{R}^1$  and  $\Gamma(\cdot)$  denote one-dimensional space and gamma function, respectively.  $\mathcal{F}_X(\cdot)$ ,  $f_X(\cdot)$ , and  $\varphi_X$  denote cumulative distribution function, its corresponding probability density function and characteristic function of an RV  $X$ .

## II. SYSTEM MODEL

A typical V2V communication scenario has been shown in Fig. 1. We consider one-way double lane highway road wherein communication link either RF or VLC exists between Vehicle A and B, whereas vehicles in another lane acts as interferers (say, for instance Vehicle C and D are acting as interferers).

Vehicle B is the transmitter which is trying to communicate information (for instance, speed of vehicle, traffic direction or warning messages) with Vehicle A which acts as receiver. The location of VLC transmitter and receiver in Vehicle A and B is shown in Fig. 2. The location of photodetector may be chosen nearby vehicle headlamp/taillight. It is assumed that Vehicle B has low beam OEM LED headlights of a Toyota Corolla Altis (Taiwan model, 2015) whose received illumination pattern has been shown in Fig. 3 based on empirical measurements obtained from [28]. All the vehicles use the same frequency ( $f_c$ ), bandwidth ( $B$ ) and transmit with same power ( $P_t$ ) concurrently.

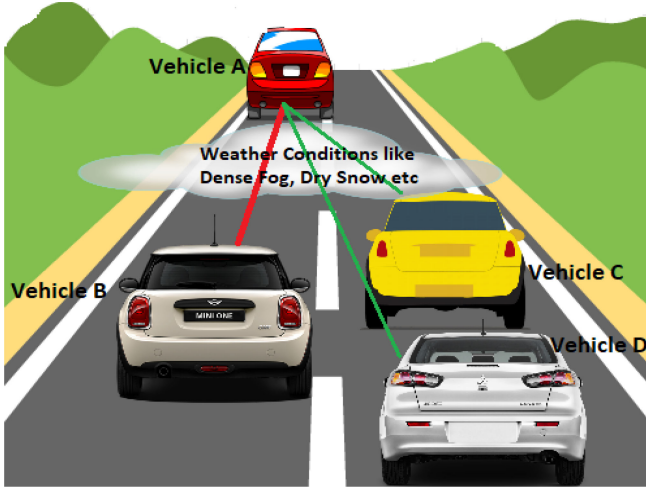


Fig. 1. System model. Here, Vehicle C and Vehicle D act as interferers (denoted by green solid line) for the dedicated communication link (denoted by red solid line) between Vehicle A and Vehicle B.

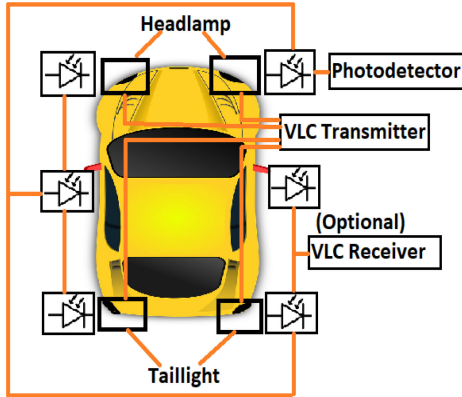


Fig. 2. Location of VLC transmitter and receiver on a typical vehicle.

We capture the randomness in geometrical distribution when the locations of interfering vehicles on a certain lane are completely independent of each other. We represent this set of vehicles as  $\Psi_{PPP}$ . We assume that the interfering vehicles are nearly aligned on the same lane and thus encounters constant lane spacing,  $L$ . Since the interfering vehicles are on the same lane and their locations are Poisson distributed, the proposed scenario resembles a uni-dimensional PPP in  $\mathbb{R}^1$  with a homogeneous congestion parameter,  $\lambda$  measured in number of vehicles per unit length. The cumulative distribution function (CDF) for spatial distribution of vehicles can be given as [25], [29]–[31]

$$F_X(x) = 1 - \exp(-\lambda x). \quad (1)$$

Apart from being more generalized and practically feasible condition, the main motivation behind utilizing PPP is to allow on an average tractable analysis of the proposed scenario by utilizing various tools of stochastic geometry. We characterize desired signal and interfering signal as signal received from desired transmitter and signals received from interferers at the typical receiver, respectively.

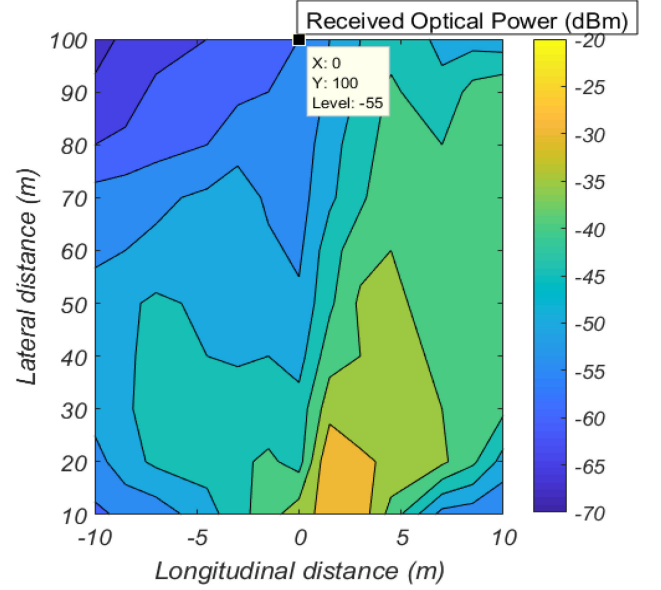


Fig. 3. OEM headlamp optical illumination pattern with receiver height of 0.7 m. The values in the plots represent the received optical power and are in dbm.

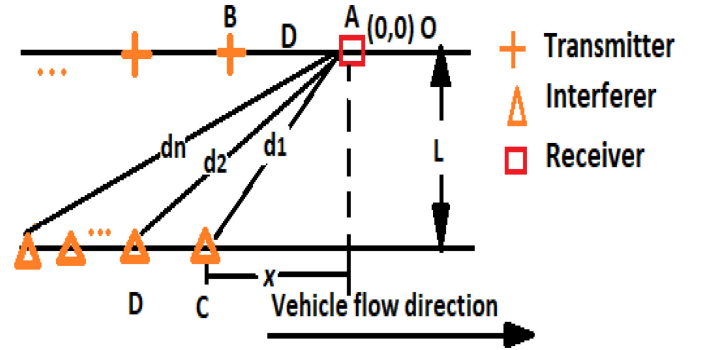


Fig. 4. Simplified geometrical layout. Vehicle a is assumed to be located at the origin  $O$ . Here,  $d$  denotes distance between legitimate vehicle and receiver.

#### A. Statistics of Mean Interference

A more generalized and simplified geometrical layout of proposed scenario has been shown in Fig. 4. It is assumed that Vehicle A is located at the origin  $O$ . Here,  $L$ ,  $x$ , and  $d_n$  denote the interlane spacing, the horizontal distance of interferer from origin  $O$  and the distance of  $n$ th interferer to Vehicle A, respectively. For outdoor VLC applications with piece-wise path loss model, the average received optical power at a typical receiver which is located at a distance,  $D$  from a legitimate transmitter can be given as [4], [28], [32], [33]

$$\bar{P}_r = \frac{(m+1)A_R}{2\pi D^\gamma} \cos^m(\phi) \cos(\theta_R) P_t \quad (2)$$

where  $A_R$ ,  $\gamma$ ,  $\phi$ , and  $\theta_R$  denote the area of PD, the path loss exponent, the angle of irradiance, and the angle of arrival (AoA), respectively. Here,  $m$  is the order of the Lambertian model and is given by  $m = -\frac{\ln(2)}{\ln(\cos(\phi_{\frac{1}{2}}))}$ . Kindly note that (2) gives the average

received optical power from legitimate transmitter (Vehicle B) at typical receiver (Vehicle A) with major line-of-sight (LOS) component. It has been demonstrated by Zeng *et al.* [34] that even the strongest diffuse component is at least 7-dB lower than the weakest LOS component. Hence, only the LOS path is taken into account for getting desired signal at typical receiver. The aggregate interference from all the interferers at the receiver can be given as sum of all the optical power received from  $N$  interferers as

$$\mathcal{I} = \sum_{x \in \Psi_{\text{PPP}}} \frac{(m+1)A_R}{2\pi(L^2+x^2)^{\frac{\gamma}{2}}} \alpha_x \cos^m(\phi_x) \cos(\theta_x) P_t. \quad (3)$$

In the above-mentioned equation, a statistical fading process is incorporated in the model which is given as a random variable ( $\alpha$ ). It represents multipath fading coefficient associated with particular  $n$ th interferer. This randomness in channel is mainly caused by multipath reflections from buildings, surrounding environment, and other vehicles. The channel model for outdoor VLC link can be formulated based on Poisson distribution of location of vehicles. From Fig. 4, we can find euclidean distance in terms of interlane spacing ( $L$ ) and horizontal distance ( $x$ ) as  $\cos(\theta_R) = \cos(\phi) = \frac{x}{\sqrt{(L^2+x^2)}}$ . Hence, equation (3) can be rewritten as

$$\mathcal{I}_{\text{VLC}} = \sum_{x \in \Psi_{\text{PPP}}} \frac{(m+1)A_R}{2\pi(L^2+x^2)^{\frac{\gamma}{2}}} \alpha_x \frac{x^{m+1}}{(L^2+x^2)^{\frac{m+1}{2}}} P_t. \quad (4)$$

In order to evaluate the mean of interference power ( $\bar{\mathcal{I}}_{\text{VLC}}$ ), the Campbell theorem<sup>2</sup> is applied to calculate the sum over a homogeneous PPP

$$\bar{\mathcal{I}}_{\text{VLC}} = \mathbb{E}_{\alpha} \mathbb{E}_{\Psi_{\text{PPP}}} \left[ \sum_{x \in \Psi_{\text{PPP}}} \mu_1 \alpha_x P_t \frac{x^{(m+1)}}{(L^2+x^2)^{\frac{m+\gamma+1}{2}}} \right] \quad (5)$$

where  $\mu_1 = \frac{(m+1)A_R}{2\pi}$ ,  $\mathbb{E}_{\alpha}$  is the expectation over the statistical fading channel and  $\mathbb{E}_{\Psi_{\text{PPP}}}$  is the geometric expectation taken over all possible realizations of the locations of interferers,  $\Psi = \{x_1, x_2, \dots\} \subset \mathbb{R}^1$  with intensity,  $\lambda$ . For our analysis, we assume that each propagation channels have an independent and identical (i.i.d) distribution and is independent from the defined geometrical point process. With no loss of generality, it is assumed that the average channel gain is unity, i.e.,  $\mathbb{E}[\alpha] = 1$ , and there exists sufficiently large number of interferers, thus (5) can be further be simplified as

$$\begin{aligned} \bar{\mathcal{I}}_{\text{VLC}} &\stackrel{(a)}{=} \mathbb{E}_{\Psi_{\text{PPP}}} \left[ \sum_{x \in \Psi_{\text{PPP}}} \mu_1 P_t \frac{x^{(m+1)}}{(L^2+x^2)^{\frac{m+\gamma+1}{2}}} \right] \\ &\stackrel{(b)}{=} \int_0^{\infty} \mu_1 P_t \frac{x^{(m+1)}}{(L^2+x^2)^{\frac{m+\gamma+1}{2}}} \lambda dx \end{aligned}$$

<sup>2</sup>Campbells theorem transforms an expectation taken over a random sum for the point process (PP) to an integral involving the PP intensity function [22]. More specifically, for a homogeneous PPP  $\Psi_{\text{PPP}}$  with intensity  $\lambda$  and a measurable function  $f: \mathbb{R}^d \rightarrow \mathbb{R}$ , the sum of  $f$  over the homogeneous PPP is given by [22, Th. 4.6]

$$\mathbb{E} \left[ \sum_{x \in \Psi_{\text{PPP}}} f(x) \right] = \lambda \int_{\mathbb{R}^d} f(x) dx.$$

$$\begin{aligned} &\stackrel{(c)}{=} \frac{\lambda P_t \mu_1 L^2 (m+2) \Gamma(\frac{\gamma-1}{2}) \Gamma(\frac{m+2}{2})}{4 L^{(m+1+\gamma)} \Gamma(\frac{m+\gamma+1}{2})} \\ &= \lambda k' \end{aligned} \quad (6)$$

where  $k' = \frac{P_t \mu_1 L^2 (m+2) \Gamma(\frac{\gamma-1}{2}) \Gamma(\frac{m+2}{2})}{4 L^{(m+1+\gamma)} \Gamma(\frac{m+\gamma+1}{2})}$ . Step (a) follows the assumption that each V-VLC propagation channels have an i.i.d distribution and is independent from defined geometrical point process. The distance distribution ( $f_X(x)$ ) is assumed to be Poisson distributed and thus step (b) follows from Campbell theorem. Step (c) has been obtained using 3.241 [35].

In case of RF-based V2V, the interference at the receiver assuming free space path loss propagation model can be given as sum of all the power received from all the interferers as

$$\mathcal{I}_{\text{RF}} = \sum_{x \in \Psi_{\text{PPP}}} P_t G_t G_r \ell h_x \|L^2 + x^2\|^{-\frac{\alpha}{2}}. \quad (7)$$

Here,  $\ell = \frac{c^2}{(4\pi)^2 f_0^2}$ ;  $c$  is speed of light and  $f_0$  is carrier frequency. In the above expression,  $\alpha$ ,  $G_t$ , and  $G_r$  are the path loss exponent, the antenna gains for transmitter and receiver, respectively [36]. We assume that the received signal amplitude in RF-based V2V channel follows Rayleigh probability distribution function (PDF). Given a RF link, fading gain ( $h_x$ ) is either an exponential r.v. of unit mean in the case of Rayleigh fading, or is set to 1 when no channel fading is considered.

Using similar steps (4)–(6) and assumptions as before, the average interference ( $\bar{\mathcal{I}}_{\text{RF}}$ ) at receiver for RF-based V2V can be given in simplified form as

$$\bar{\mathcal{I}}_{\text{RF}} = \frac{\lambda \gamma_2 P_t L^{(1-\alpha)} 2\sqrt{\pi} \Gamma(\frac{\alpha+3}{2})}{(\alpha^2 - 1) \Gamma(\frac{\alpha}{2})}. \quad (8)$$

where  $\gamma_2 = \frac{G_t G_r c^2}{(f_0)^2 (4\pi)^2}$ .

Apart from interference in VLC-based V2V, there are other major sources of noise, namely, thermal and shot noise. The total noise variance ( $\sigma_{\text{total}}^2$ ) can be expressed as

$$\sigma_{\text{total}}^2 = \sigma_{\text{shot}}^2 + \sigma_{\text{thermal}}^2 \quad (9)$$

where  $\sigma_{\text{shot}}^2$  and  $\sigma_{\text{thermal}}^2$  denote shot and thermal noise variances, and are given as [28]

$$\sigma_{\text{shot}}^2 = 2e\mathcal{R}P_r B_s \quad (10)$$

$$\sigma_{\text{thermal}}^2 = 4 \left( \frac{K_B T_k}{R_L} \right) B_s \quad (11)$$

where  $\mathcal{R}$  is the responsivity of the PD,  $e$  is the electron charge,  $P_r$  is the average optical power received from vehicle headlamp,  $K_B$  is Boltzmann's constant,  $T_k$  is the absolute temperature in Kelvin, and  $R_L$  is load resistance given as 10 k $\Omega$ . In this article, the optical receiver is assumed to be a nonimaging PIN PD, which is equipped at the rear end of the vehicle. The PD can be modeled using its effective collection area  $A_{\text{Reff}}$ , which is given as [37]

$$A_{\text{Reff}} = \begin{cases} A_R \cos(\theta_R); & \text{if } 0 \leq \theta_R \leq \Psi_{\text{FOV}} \\ 0; & \text{if } \theta_R > \Psi_{\text{FOV}} \end{cases} \quad (12)$$

where  $\Psi_{\text{FOV}}$  denotes PD's field of view (FOV).

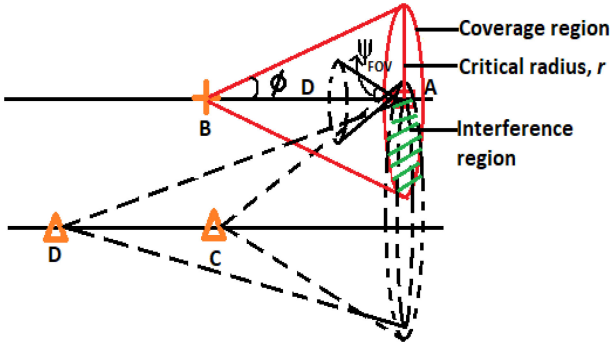


Fig. 5. Reference scenario illustrating coverage and interference region using VLC attocells. Here,  $R$  and  $D$  denotes radius of VLC attocell under coverage region of desired vehicle and communication-range, respectively.

Typically, the received signal as well as the interference model considers full FOV of  $180^\circ$  at the PD receiver which leads to a worst-case bound on the interference. Nonetheless, for a typical receiver, the received interference power as well as the received signal power heavily depends on the FOV of the receiver. Moreover, considering a full FOV of the PD assumes that the interferers are always within the FOV of the desired receiver, which may not be true and hence overestimate the total interference for the given scenario. It can be inferred from (6) that the radiation power received by the PD when PDs FoV is  $180^\circ$  is indeed a worst-case scenario. In order to show the reduced effect of interference and increase the communication range from desired vehicle, we introduced the correction function,  $C(\theta_R)$  at the receiver, which implies that the interferers that are located within PDs FOV will only be considered. Correction function  $C(\theta_R)$  can be expressed in terms of PDs FoV as

$$C(\theta_R) = \begin{cases} 1; & \text{if } 0 \leq \theta_R \leq \Psi_{\text{FOV}} \\ 0; & \text{if } \theta_R > \Psi_{\text{FOV}}. \end{cases} \quad (13)$$

The above scenario can be best visualized in the form of Fig. 5 which clearly depicts that reducing PD's FOV can significantly reduce the effect of interference caused by interferers from other lane. Like small cell concept for indoor RF scenario, the VLC attocell concept can be applied for outdoor scenarios as well [38], [39]. In fact, the critical radius<sup>3</sup> ( $r$ ) of VLC attocell for desired vehicle with communication range ( $D$ ) can be defined as the radius beyond which the effect of interference is less pronounced (i.e.,  $P_r > \bar{I}_{\text{VLC}}$ ). The critical radius can be computed as

$$\frac{C(\theta_R)(m+1)A_R}{2\pi D^\gamma} \frac{D^{(m+1)}}{(D^2 + r^2)^{\frac{(m+1)}{2}}} P_t > C(\theta_R)\lambda k' \quad (14)$$

(14) can be rewritten as

$$r < \left\{ \left[ \frac{(m+1)A_R P_t}{\lambda k' D^\gamma} - 1 \right] \frac{2D^2}{(m+1)} \right\}^{\frac{1}{2}} \quad D \gg r. \quad (15)$$

<sup>3</sup>The notion of critical radius in general contains the effect of PD's FOV variation.

The average SINR for V-VLC at the receiver can be given as

$$\text{SINR}_{\text{VLC}} = \frac{(\mathcal{R}P_r)^2}{\sigma_{\text{total}}^2 + \bar{I}_{\text{VLC}}} \quad (16)$$

where  $\bar{I}_{\text{VLC}}$  represents noise due to interference from interferer [40]. The theoretical bit error rate (BER) of ON-OFF keying (OOK) in an additive white Gaussian noise (AWGN) channel is given as [2]

$$\text{BER} = Q(\sqrt{\text{SINR}}) = Q\left(\frac{\mathcal{R}P_r}{\sqrt{\sigma_{\text{total}}^2 + \bar{I}_{\text{VLC}}}}\right). \quad (17)$$

The average SINR for V-RF at the receiver is given as [41]

$$\text{SINR}_{\text{RF}} = \frac{P_r}{\sigma_N^2 + \bar{I}_{\text{RF}}} \quad (18)$$

where  $\sigma_N^2$  denotes thermal noise power at RF receiver.

### B. Cumulative Distribution Function of Interference

The cumulative distribution function of interference ( $F_I(x)$ ) is defined as the probability that interference power is below than a certain minimum threshold level. At the receiver, it is indeed important that interference power should be as minimum as possible for a signal to be decoded correctly.

In order to evaluate the statistical behavior of the interference, we first obtain its characteristics function (CF) denoted as  $\varphi_I$  and then evaluate its CDF denoted as  $\mathcal{F}_I(x)$ . The CF of a random variable  $X$  is defined as  $\mathbb{E}[e^{j\omega X}]$ . For the proposed scenario, the characteristic function can be expressed as

$$\begin{aligned} \varphi_I(\omega) &= \mathbb{E}[e^{j\omega I}] \\ &= \mathbb{E}_{\alpha_x} \mathbb{E}_{x \in \Psi_{\text{PPP}}} \left[ \exp\left(j\omega \sum_{x \in \Psi_{\text{PPP}}} \mu_1 P_t \alpha_x \frac{x^{m+1}}{(L^2 + x^2)^{\frac{m+\gamma+1}{2}}}\right) \right] \\ &= \mathbb{E}_{x \in \Psi_{\text{PPP}}} \left[ \prod_{x \in \Psi_{\text{PPP}}} \mathbb{E}_{\alpha_x} \exp\left(j\omega \mu_1 P_t \alpha_x \frac{x^{m+1}}{(L^2 + x^2)^{\frac{m+\gamma+1}{2}}}\right) \right]. \end{aligned} \quad (19)$$

The previous step comes from the fact that the channel fading random variable ( $\alpha$ ) is assumed to be independent of the geometrical stochastic process ( $\Psi_{\text{PPP}}$ ). The probability generating functional (PGFL)<sup>4</sup> for function  $f(x)$  for homogeneous PPP over region of interest,  $\mathcal{R}$  can be given as [22, Th. 4.9]

$$\mathbb{E} \left[ \prod_{x \in \Psi_{\text{PPP}}} f(x) \right] = \exp \left( -\lambda \int_{\mathcal{R}} [1 - f(x)] dx \right). \quad (20)$$

<sup>4</sup>The PGFL can be visualized as an equivalent for point process of the moment generating function or characteristic function (that provide an alternative description of random variables). It enables to compute the Laplace transform (LT) of random variables of the form  $F = \sum_{X_i \in \Psi_{\text{PPP}}} g(X_i)$ . Mathematically, LT of such function can be given as

$$\mathcal{L}(s) = \mathbb{E} \left[ \exp \left( -s \sum_{X_i \in \Psi} g(X_i) \right) \right] = \mathbb{E} \left[ \prod_{X_i \in \Psi} e^{-s g(X_i)} \right].$$

Using (20), (19) can be rewritten as

$$\varphi_{\mathcal{I}}(\omega) = \exp \left( -\mathbb{E}_{\alpha_x} \int_0^{\infty} \left[ 1 - \exp \left( \frac{j\omega\alpha_x\mu_1 P_t x^{m+1}}{(L^2 + x^2)^{\frac{m+\gamma+1}{2}}} \right) \right] \lambda dx \right). \quad (21)$$

The above integral can be numerically evaluated in order to obtain the CDF using Gil-Pelaez's inversion theorem [42]

$$F_{\mathcal{I}}(x) = \frac{1}{2} - \frac{1}{\pi} \int_0^{\infty} \frac{1}{\omega} \Im [\varphi_{\mathcal{I}}(\omega) e^{-j\omega x}] d\omega. \quad (22)$$

For sake of simplicity, the interlane distance,  $L$  with respect to the longitudinal stretch of the road is ignored. Without loss of generality, we further simplify the above characteristic function by setting the value of path loss exponent ( $\gamma = 2$ ) and as there is no channel fading in case of V-VLC, thus (21) reduces to a simplified form as

$$\begin{aligned} \varphi_{\mathcal{I}}(\omega) &= \exp \left( -\mathbb{E}_{\alpha_n} \left[ \lambda \Gamma \left( 1 - \frac{1}{\gamma} \right) (-j\alpha_n \mu_1 P_t \omega)^{\frac{1}{\gamma}} \right] \right) \\ &= \exp \left( -\sqrt{-j\pi\mu_1 P_t \omega \lambda^2} \right). \end{aligned} \quad (23)$$

Equation (23) can be compared with a tractable Levy-distribution having a CF and a CDF of the form

$$\begin{aligned} \varphi(\omega) &= e^{(j\mu\omega - \sqrt{-2jc\omega})} \\ F_X(x) &= \xi_c \left( \sqrt{\frac{c}{2(x-\mu)}} \right) \end{aligned} \quad (24)$$

where  $\mu$  and  $c$  are the location parameter and the scale parameter, respectively. By comparing (23) with (24), we can conclude that the function follows a Levy distribution with CDF:

$$F_{\mathcal{I}_{\text{VLC}}}(x) = \xi_c \left( \sqrt{\frac{\pi\lambda^2\mu_1 P_t}{4x}} \right). \quad (25)$$

Using similar steps (18)–(24) and assumptions as before, the expression for interference cumulative distribution function for RF-based V2V can be given as

$$F_{\mathcal{I}_{\text{RF}}}(x) = \xi_c \left( \sqrt{\frac{\pi\lambda^2\gamma_2 P_t}{4x}} \right). \quad (26)$$

The performance of proposed scenario has been evaluated in terms of probability of successful transmission,  $P_s$  as performance metric for three different traffic scenarios viz., dense, medium, and sparse traffic scenario.

### III. PROBABILITY OF SUCCESSFUL TRANSMISSION

For a given modulation and coding scheme (MCS), treating interference as noise, say for instance, by using a simple linear receiver, a well-accepted model for packetized transmissions is considered successful if the SINR exceeds a certain threshold ( $\zeta$ ). The probability of successful transmission ( $\mathcal{P}_s$ ) is formally defined as the probability that SINR is greater than a certain minimum threshold level. Its complement is outage probability.

The SINR can be given as

$$SINR = \frac{S}{\mathcal{I}_{\{\text{VLC,RF}\}} + \sigma_t^2} \quad (27)$$

where  $\sigma_t^2$  denotes the noise variance. Accordingly, we formulate the probability of successful packet transmission as

$$\begin{aligned} P_s &= \mathbb{P}(SINR \geq \zeta) \\ &= \mathbb{P} \left( \mathcal{I}_{\{\text{VLC,RF}\}} \leq \frac{S}{\zeta} - \sigma_t^2 \right) \\ &= \mathcal{F}_{\mathcal{I}} \left( \frac{S}{\zeta} - \sigma_t^2 \right). \end{aligned} \quad (28)$$

Thus, the probability of successful packet transmission for V-VLC can be given as

$$P_s = \xi_c \left( \sqrt{\frac{\pi\lambda^2\mu_1 P_t}{4 \left( \frac{S}{\zeta} - \sigma_t^2 \right)}} \right). \quad (29)$$

For dense traffic scenario, interference becomes the limiting performance factor rather than the noise variance and hence, noise variance may be ignored. Hence, (29) reduces to

$$P_s = \xi_c \left( \sqrt{\frac{\pi\lambda^2\mu_1 P_t \zeta}{4S}} \right). \quad (30)$$

We investigate the probability of successful packet transmission for V-RF communication on free-space propagation model with no channel fading as well as Rayleigh-fading cases.

#### A. No Channel Fading With Path Loss Exponent, $\alpha = 2$

In case of no-channel fading, the presented framework offers a closed-form expression of probability of successful transmission<sup>5</sup> which is given as

$$P_s = \xi_c \left( \sqrt{\frac{\pi\lambda^2\gamma_2 P_t \zeta}{4S}} \right). \quad (31)$$

#### B. Rayleigh Fading Case

In this case, we consider a higher path-loss exponent and Rayleigh fading on the interfering signals as worst-case scenario of the multipath-induced random fluctuations in the received power. The probability of successful transmission ( $\mathcal{P}_s$ ) can be given as

$$P_s = \mathcal{L}_{\text{IRF}} \left( \frac{\zeta}{P_t G_t G_r \ell D^{-\alpha}} \right) \exp \left( -\frac{\zeta \sigma_t^2}{P_t G_t G_r \ell D^{-\alpha}} \right) \quad (32)$$

where  $\mathcal{L}(\cdot)$  stands for Laplace transform which is given as

$$\mathcal{L}_{\text{IRF}} \left( \frac{\zeta}{P_t G_t G_r \ell D^{-\alpha}} \right) = \exp \left( -\lambda(\zeta)^{\frac{1}{\alpha}} D \frac{\pi}{\alpha} \csc \left( \frac{\pi}{\alpha} \right) \right). \quad (33)$$

*Proof:* Please refer to the Appendix.

<sup>5</sup>The expression has been derived in same way as discussed before for V-VLC scenario.

TABLE I  
SYSTEM MODEL PARAMETERS

Parameter	Symbol	Value
Lambertian Order	$m$	2, 4 and 6
PD active detection area	$A_d$	$1.2 \text{ mm}^2$
Transmission power for RF	$P_t$	33 dBm [34]
Transmission power for VLC	$P_t$	36.5 dBm
Responsivity of the PD	$\mathcal{R}$	0.54 A/W [2]
Electronic charge	$e$	$1.6 \times 10^{-19} \text{ C}$
Noise variance	$\sigma_t^2$	-99 dBm
Boltzmann's constant	$K_B$	$1.38 \times 10^{-23} \text{ J/K}$
Absolute temperature	$T_k$	298° K
System Bandwidth	$B_s$	2 MHz [2]
Transmitter antenna gain	$G_t$	3dBi
Receiver antenna gain	$G_r$	3dBi
Visibility parameter light fog	$V$	0.1 km
Visibility parameter dense fog	$V$	0.05 km
Attenuation coefficient under light fog	$\beta$	39.4 dB/km [45]
Attenuation coefficient under dense fog	$\beta$	78.8 dB/km [45]
Attenuation coefficient under dry snow (snow rate=10 mm/hr)	$\beta_{dry\ snow}$	131 dB/km [45]
Inter-lane spacing	$L$	10 m

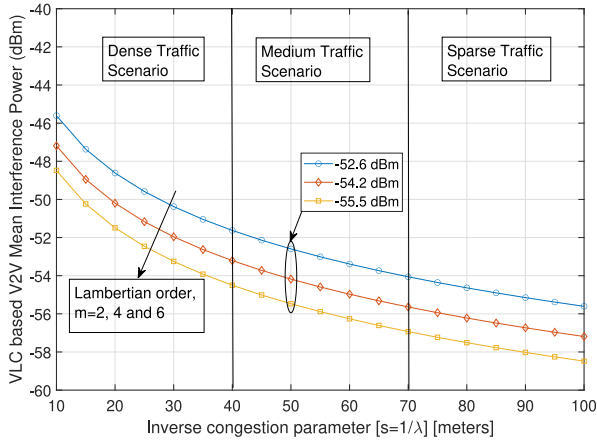


Fig. 6. Mean interference variation with inverse congestion parameter for V-VLC with Lambertian Order,  $M = 2, 4,$  and  $6$  when the FOV of receiver is  $180^\circ$ .

#### IV. SIMULATION RESULTS AND ANALYSIS

The system model parameters used in the analysis are summarized in Table I. Based on (6) and (8), it can be noted that the mean interference value for both V-VLC and V-RF communication varies linearly with congestion parameter ( $\lambda$ ). In traffic flow theory, space headway ( $s$ ) is defined as horizontal distance between vehicles (in metres). The space headway is related to congestion parameter as  $s = \frac{1}{\lambda}$  [43]. Hence, space headway can also be referred as inverse congestion parameter.

It can be noted from Fig. 6 that with space headway of 50 m (medium traffic scenario), the mean interference value for V-VLC with Lambertian order  $m = 2, 4,$  and  $6$  are  $-52.6, -54.2,$  and  $-55.5$  dBm, respectively. Further, with increasing value of Lambertian order,  $m$  from 2 to 6, the interference power for V-VLC decreases indicating that the vehicles with narrower light

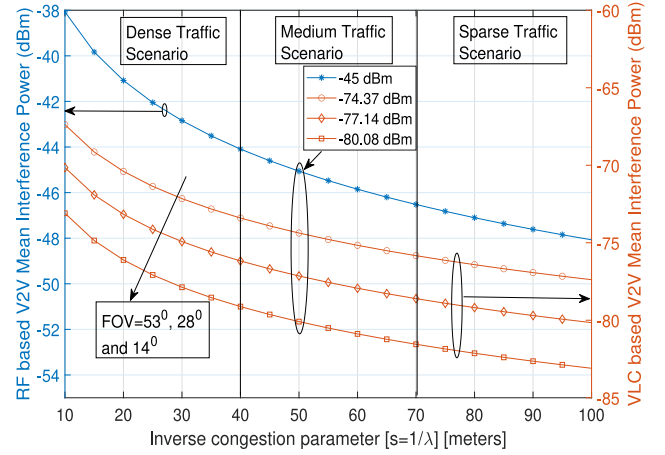


Fig. 7. Mean interference variation with inverse congestion parameter for V-RF communication ( $\alpha = 2$ ) and V-VLC with Lambertian Order,  $M = 4$  with different FOV of receiver ( $53^\circ, 28^\circ,$  and  $14^\circ$ ).

beam has lower impact on the desired communication link between Vehicle A and B as compared to vehicles with wider beam. For our analysis, the average optical transmit power is taken to be 36.5 dBm for a typical Toyota Corolla Altis headlamp module. The transmission power for V-RF communication is taken to be 33 dBm which is maximum allowable transmission power given by federal communications commission (FCC) [44]. The impact of reducing the FOV of the receiver on the level of interference experienced at the typical receiver can be well observed from Fig. 7. The mean interference value for V-VLC with Lambertian order<sup>6</sup>  $m = 4$  when space headway between vehicles is 50 m are  $-74.37, -77.14,$  and  $-80.08$  dBm with receiver's FOV of  $53^\circ, 28^\circ,$  and  $14^\circ$ , respectively. The mean interference for V-RF communication when space headway between interferer is 50 m is  $-45$  dBm.

Fig. 8 shows modified OEM headlamp optical radiation pattern with receiver height of 0.7 m with interference under worst-case scenario (FOV of receiver =  $180^\circ$ ) and space headway between interferers is 20 m. The average received optical power at a distance of 100 m from transmitter degrades by 10 dB as compared to radiation pattern observed without considering the impact of interference. Fig. 9 shows the impact of various environmental deterrents on OEM headlamp optical radiation pattern based on [17] and [46]. Table II shows the impact of interference as well as various environmental deterrents on average received optical power with receiver height of 0.7 m at a distance of 100 m from location of headlamp. As compared to normal atmospheric conditions, the optical power loss<sup>7</sup> at a distance of 100 m from transmitter under dry snow condition reduces by 23 dB taking into consideration the effect of interference as well as the environmental deterrent.

<sup>6</sup>The Lambertian order  $m = 4$  best describes the closest approximation of vehicle radiation pattern and thus has been chosen for our analysis.

<sup>7</sup>Power loss has been calculated with respect to average optical power received at a distance of 100 m from transmitter without taking into consideration the impact of interference and environmental deterrents.

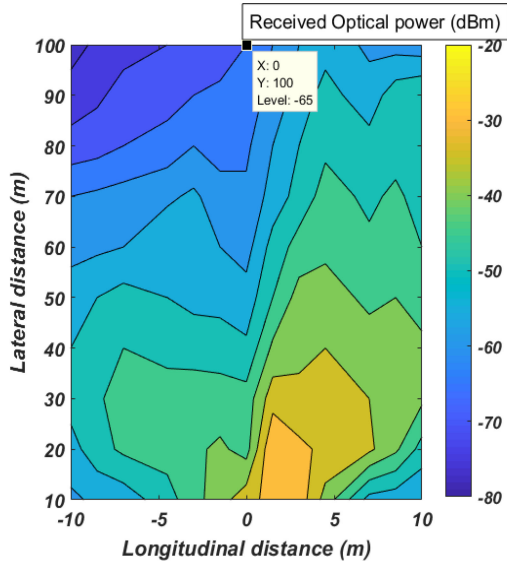


Fig. 8. OEM headlamp optical radiation pattern with receiver height of 0.7 m with interference under worst-case scenario when space headway between interferers is 20 m.

TABLE II  
AVERAGE RECEIVED OPTICAL POWER FOR V-VLC IN PRESENCE OF INTERFERENCE WHEN SPACE HEADWAY BETWEEN INTERFERER IS 20 m UNDER DIFFERENT ENVIRONMENTAL DETERRENTS AT A DISTANCE OF 100 m FROM TRANSMITTER

S.No.	V2V Communication	Received power (dBm)	Power loss (dB)
1	V-VLC under normal atmospheric	-65 dBm	10 dB
2	V-VLC under light fog	-69 dBm	14 dB
3	V-VLC under dense fog	-73 dBm	18 dB
4	V-VLC under dry snow	-78 dBm	23 dB

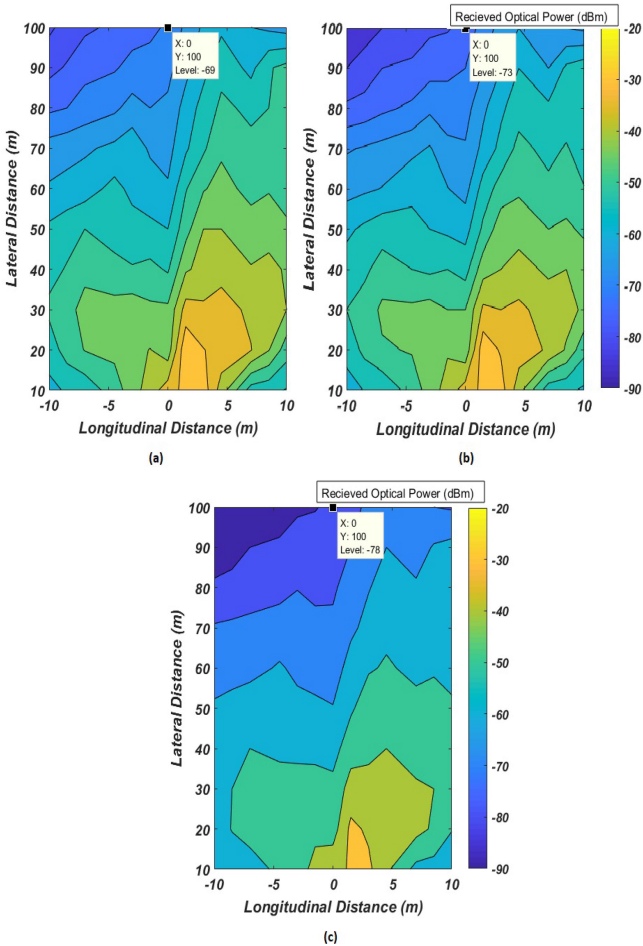


Fig. 9. OEM headlamp optical radiation pattern with receiver height of 0.7 m with interference when space headway between interferers is 20 m. (a) Light fog ( $V=0.1$  Km). (b) Dense fog ( $V=0.05$  Km). (c) Dry snow condition (snow rate=10 Mm/hr).

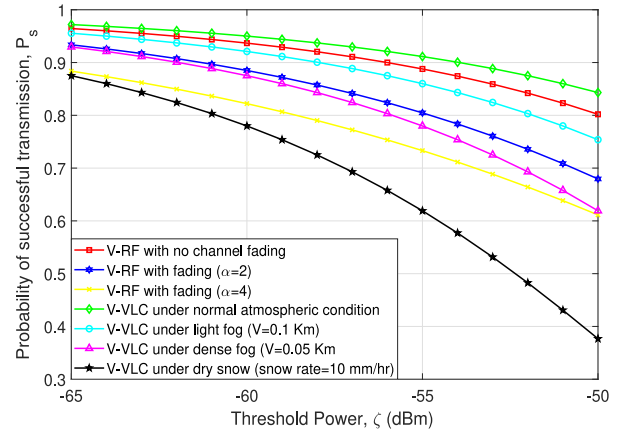


Fig. 10. Probability of successful transmission over a range of threshold power for sparse traffic scenario when inverse congestion parameter is 50 m.

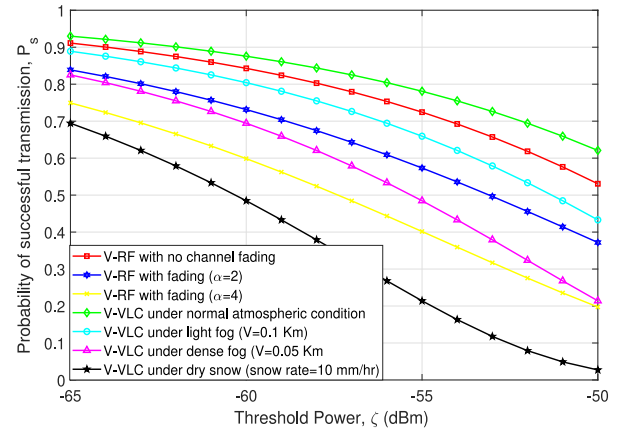


Fig. 11. Probability of successful transmission over a range of threshold power for medium traffic scenario when inverse congestion parameter is 20 m.

Figs. 10–12 show probability of successful transmission variation over a range of threshold power for V-RF and V-VLC under various environmental deterrents for three different traffic scenarios viz., sparse, medium, and dense traffic. It can be observed that irrespective of traffic scenario, the probability of successful transmission for V-VLC communication under normal atmospheric condition outperforms V-RF communication

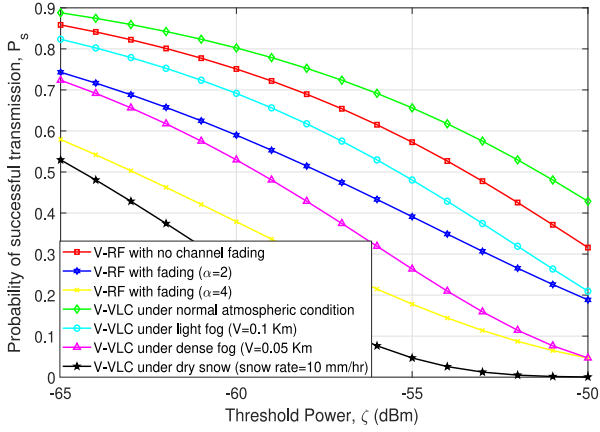


Fig. 12. Probability of successful transmission over a range of threshold power for dense traffic scenario when inverse congestion parameter is 12.5 m.

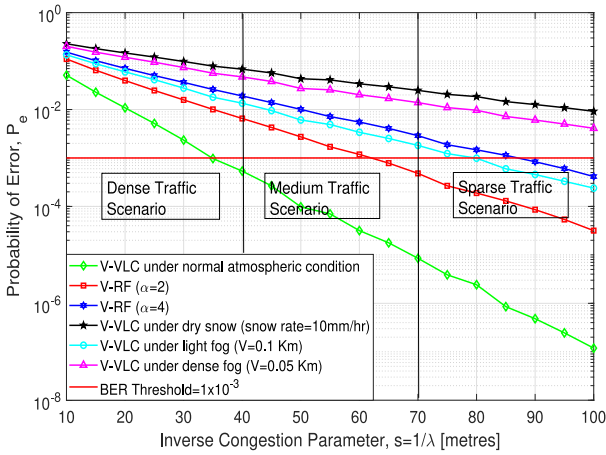


Fig. 13. Comparison for probability of error,  $p_e$  variation with inverse congestion parameter for V-RF and V-VLC when distance between vehicle A and B for VLC and RF is assumed to be 35 m.

for a given threshold power. However, it is also worth noting here that for a given threshold power, V-RF communication under no fading conditions outperforms V-VLC when environmental deterrents such as light fog, dense, and dry snow conditions are considered. Interestingly, the performance of V-VLC under light fog condition is comparatively better than the performance of V-RF communication under Rayleigh fading conditions with path loss exponent,  $\alpha$  of 2 or 4. With threshold power of  $-65$  dBm, the performance of V-VLC under dry snow condition falls by 40% as compared to normal weather conditions under dense traffic scenario when inverse congestion parameter is 12.5 m. This is primarily due to high attenuation in the average optical power received under dry snow condition. Kindly note that the proposed article does not take into account scheduling for vehicular transmission, which indeed resulted in lower probability of successful transmission for some curves, especially dense traffic scenario. The benefit of employing various MAC protocols in order to facilitate scheduled vehicular transmission will be considered as a subject of future work.

TABLE III  
PERFORMANCE OF V-RF COMMUNICATION AND V-VLC UNDER DIFFERENT ENVIRONMENTAL DETERRENTS IN PRESENCE OF INTERFERENCE WITH BER OF  $1 \times 10^{-3}$  AS PERFORMANCE BENCHMARK

S.No.	V2V Communication	Dense Traffic scenario	Medium Traffic scenario	Sparse Traffic scenario
1	V-VLC under normal atmospheric	✓	✓	✓
2	V-RF communication ( $\alpha=2$ )	✗	✓	✓
3	V-RF communication ( $\alpha=4$ )	✗	✗	✓
4	V-VLC under light fog	✗	✗	✓
5	V-VLC under dense fog	✗	✗	✗
6	V-VLC under dry snow	✗	✗	✗

Based on empirical calculations using (10) and (11), the shot noise due to received optical power and thermal noise when distance between Vehicle A and Vehicle B is 35 m can be found to be  $-187$  and  $-145$  dBm, respectively. The mean interference for VLC-based V2V with Lambertian order,  $m=4$  is  $-68$  dBm when space headway between interferers is 100 m (sparse traffic). Hence, for the proposed scenario, the thermal noise and shot noise may be neglected as compared to mean interference experienced from interferers ( $\bar{I}_{VLC} \gg \sigma_{total}^2$ ) which is the only major source that severely impacts the performance of V-VLC. Fig. 13 gives a comparison for probability of error ( $P_e$ ) variation with inverse congestion parameter for V-RF and V-VLC when distance between Vehicle A and B for VLC as well as RF scenario is assumed to be 35 m.

With BER threshold of  $1 \times 10^{-3}$  as a performance benchmark, V-VLC under normal atmospheric condition typically supports vehicular density upto 29 vehicles/km, while V-RF communication can support only 16 vehicles/km.

Further, it can be inferred from Table III that V-VLC under normal atmospheric conditions can support dense traffic scenario, while V-RF communication serves as better alternative option for communication under different environmental deterrents such as light fog, dense fog, and dry snow conditions supporting medium as well as sparse traffic scenario. It is worth noting here that V-VLC can be more reliable option over V-RF for dense traffic scenario under different environmental deterrents by employing various scheduling-based MAC protocols which are a part of future scope of this article.

## V. CONCLUSION

The proposed article characterized various aspects of stochastic behavior of interference by modeling location of road vehicles as a spatial PPP. This article is also precise in terms of capturing the impact of reducing FOV of receiver on the level of interference experienced from interferers. The performance of conventional V-RF and V-VLC under various environmental deterrents viz., light fog, dense fog, and dry snow conditions

has been investigated and evaluated in terms of probability of successful transmission as a performance metric. We have also illustrated OEM headlamp illumination patterns in presence of interference under above environmental deterrents. Irrespective of any traffic scenario, the performance of V-VLC communication under normal atmospheric condition always outperforms V-RF communication. However, the performance of V-RF communication is comparatively better than V-VLC under various environmental deterrents. The proposed result motivates the benefit of employing RF-based or VLC-based V2V communication which can cater for different environmental deterrents, thus serving as a better alternative option to meet diverse application needs for future intelligent transportation system.

#### APPENDIX

The probability of successful transmission for V-RF communication with Rayleigh fading can be computed as

$$\begin{aligned}
 P_s &= \mathbb{P}(SINR \geq \zeta) \\
 &= \mathbb{P}\left(\frac{P_t G_t G_r \ell h_x D^{-\alpha}}{I_{RF} + \sigma_t^2} > \zeta\right) \\
 &= \mathbb{E}_{I_{RF}} \left[ \mathcal{P}\left(h_x > \frac{\zeta}{P_t G_t G_r \ell D^{-\alpha}} (I_{RF} + \sigma_t^2)\right) \right] \\
 &= \exp\left(-\frac{\zeta \sigma_t^2}{P_t G_t G_r \ell D^{-\alpha}}\right) \mathbb{E}_{I_{RF}} \left[ \exp\left(-\frac{\zeta I_{RF}}{P_t G_t G_r \ell D^{-\alpha}}\right) \right] \\
 &= \mathcal{L}_{I_{RF}} \left( \frac{\zeta}{P_t G_t G_r \ell D^{-\alpha}} \right) \exp\left(-\frac{\zeta \sigma_t^2}{P_t G_t G_r \ell D^{-\alpha}}\right) \quad (34)
 \end{aligned}$$

where  $\mathcal{L}(\cdot)$  stands for Laplace transform which is given as

$$\begin{aligned}
 \mathcal{L}_{I_{RF}}(s) &= \mathbb{E}[\exp(-s I_{RF})] \\
 &= \mathbb{E} \left[ \prod_x \exp(-s P_t G_t G_r \ell h_x ||x||^{-\alpha}) \right] \\
 &\stackrel{(a)}{=} \mathbb{E}_x \left[ \prod_x \mathbb{E}_{h_x} \{ \exp(-s P_t G_t G_r \ell h_x ||x||^{-\alpha}) \} \right] \\
 &= \mathbb{E}_x \left[ \prod_x \frac{1}{1 + s P_t G_t G_r \ell ||x||^{-\alpha}} \right] \\
 &\stackrel{(b)}{=} \exp\left(-\lambda \int_0^\infty \frac{1}{1 + ||x||^\alpha / s P_t G_t G_r \ell} dx\right) \\
 &\stackrel{(c)}{=} \exp\left(-\lambda (s P_t G_t G_r \ell)^{\frac{1}{\alpha}} \int_0^\infty \frac{1}{1 + v^\alpha} dv\right) \\
 &= \exp\left(-\lambda (s P_t G_t G_r \ell)^{\frac{1}{\alpha}} \frac{\pi}{\alpha} \csc\left(\frac{\pi}{\alpha}\right)\right). \quad (35)
 \end{aligned}$$

Here, step (a) holds due to independence of fading coefficients  $h_x$  and assumes  $L \ll x$ . Step (b) uses the definition of PGFL for PPP, and step (c) involves the change of variable  $||x|| / (s P_t G_t G_r \ell)^{\frac{1}{\alpha}} \rightarrow v$ . Substituting  $s = \frac{\zeta}{P_t G_t G_r \ell D^{-\alpha}}$  yields

the desired result

$$\mathcal{L}_{I_{RF}} \left( \frac{\zeta}{P_t G_t G_r \ell D^{-\alpha}} \right) = \exp\left(-\lambda (\zeta)^{\frac{1}{\alpha}} D^{\frac{\pi}{\alpha}} \csc\left(\frac{\pi}{\alpha}\right)\right). \quad (36)$$

#### REFERENCES

- [1] Y. L. Morgan, "Notes on DSRC WAVE standards suite: Its architecture, design, and characteristics," *IEEE Commun. Surv. Tuts.*, vol. 12, no. 4, pp. 504–518, Dec. 2010.
- [2] P. Luo, Z. Ghassemlooy, H. Le Minh, E. Bentley, A. Burton, and X. Tang, "Performance analysis of a car-to-car visible light communication system," *Appl. Opt.*, vol. 54, no. 7, pp. 1696–1706, Feb. 2015.
- [3] A.-M. Cailean, B. Cagneau, L. Chassagne, V. Popa, and M. Dimian, "A survey on the usage of DSRC and VLC in communication-based vehicle safety applications," in *Proc. IEEE 21st Symp. Commun. Veh. Technol.*, Nov. 2014, pp. 69–74.
- [4] L. Cheng, W. Viriyasitavat, M. Boban, and H.-M. Tsai, "Comparison of radio frequency and visible light propagation channels for vehicular communications," *IEEE Access*, vol. 6, pp. 2634–2644, 2017.
- [5] M. Elamassie, M. Karbalayghareh, F. Miramirkhani, R. C. Kizilirmak, and M. Uysal, "Effect of fog and rain on the performance of vehicular visible light communications," in *Proc. IEEE 87th Veh. Technol. Conf. Spring*, Jun. 2018, pp. 1–6.
- [6] P. Papadimitratos, A. L. Fortelle, K. Evensen, R. Brignolo, and S. Cosenza, "Vehicular communication systems: Enabling technologies, applications, and future outlook on intelligent transportation," *IEEE Commun. Mag.*, vol. 47, no. 11, pp. 84–95, Nov. 2009.
- [7] H. Fujii, O. Hayashi, and N. Nakagata, "Experimental research on inter-vehicle communication using infrared rays," in *Proc. IEEE Conf. Intell. Veh.*, Sept. 1996, pp. 266–271.
- [8] H. Sawant, J. Tan, Q. Yang, and Q. Wang, "Using bluetooth and sensor networks for intelligent transportation systems," in *Proc. IEEE 7th Int. Conf. Intell. Transp. Syst.*, Oct. 2004, pp. 767–772.
- [9] I. Lequerica, P. M. Ruiz, and V. Cabrera, "Improvement of vehicular communications by using 3G capabilities to disseminate control information," *IEEE Netw.*, vol. 24, no. 1, pp. 32–38, Jan. 2010.
- [10] Q. Zhao, Y. Zhu, C. Chen, H. Zhu, and B. Li, "When 3G meets VANET: 3G-assisted data delivery in VANETS," *IEEE Sensors J.*, vol. 13, no. 10, pp. 3575–3584, Oct. 2013.
- [11] S. Kato, M. Hiltunen, K. Joshi, and R. Schlichting, "Enabling vehicular safety applications over LTE networks," in *Proc. IEEE Int. Conf. Connected Veh. Expo*, Dec. 2013, pp. 747–752.
- [12] P. Fernandes and U. Nunes, "Platooning with DSRC-based IVC-enabled autonomous vehicles: Adding infrared communications for ivc reliability improvement," in *Proc. IEEE Intell. Veh. Symp.*, Jun. 2012, pp. 517–522.
- [13] K. Siddiqi, A. Raza, and S. S. Muhammad, "Visible light communication for V2V intelligent transport system," in *Proc. IEEE Int. Conf. Broadband Commun. Next Gener. Netw. Multimedia Appl.*, Oct. 2016, pp. 1–4.
- [14] Y. Goto *et al.*, "A new automotive VLC system using optical communication image sensor," *IEEE photon. J.*, vol. 8, no. 3, pp. 1–17, Jun. 2016, Art. no. 6802716.
- [15] W.-H. Shen and H.-M. Tsai, "Testing vehicle-to-vehicle visible light communications in real-world driving scenarios," in *Proc. IEEE Veh. Netw. Conf.*, Nov. 2017, pp. 187–194.
- [16] Y.-H. Kim, W. A. Cahyadi, and Y. H. Chung, "Experimental demonstration of LED-based vehicle to vehicle communication under atmospheric turbulence," in *Proc. IEEE Int. Conf. Info. Commun. Technol. Convergence*, Oct. 2015, pp. 1143–1145.
- [17] Y. H. Kim, W. A. Cahyadi, and Y. H. Chung, "Experimental demonstration of VLC-based vehicle-to-vehicle communications under fog conditions," *IEEE Photon. J.*, vol. 7, no. 6, pp. 1–9, Dec. 2015, Art. no. 7905309.
- [18] A. Memedi, H.-M. Tsai, and F. Dressler, "Impact of realistic light radiation pattern on vehicular visible light communication," in *Proc. IEEE Global Commun. Conf.*, Dec. 2017, pp. 1–6.
- [19] B. Turan, O. Narmanlioglu, S. C. Ergen, and M. Uysal, "Broadcasting brake lights with MIMO-OFDM based vehicular VLC," in *Proc. IEEE Veh. Netw. Conf.*, Dec. 2016, pp. 1–7.
- [20] A. Al-Hourani, S. Kandeepan, and E. Hossain, "Relay-assisted device-to-device communication: A stochastic analysis of energy saving," *IEEE Trans. Mobile Comput.*, vol. 15, no. 12, pp. 3129–3141, Dec. 2016.
- [21] A. Al-Hourani, S. Kandeepan, and A. Jamalipour, "Stochastic geometry study on device-to-device communication as a disaster relief solution," *IEEE Trans. Veh. Technol.*, vol. 65, no. 5, pp. 3005–3017, May 2016.

- [22] M. Haenggi, *Stochastic Geometry for Wireless Networks*. Cambridge, U.K.: Cambridge Univ. Press, 2012.
- [23] J. G. Andrews, F. Baccelli, and R. K. Ganti, "A tractable approach to coverage and rate in cellular networks," *IEEE Trans. Commun.*, vol. 59, no. 11, pp. 3122–3134, Nov. 2011.
- [24] A. Al Al-Hourani and S. Kandeepan, "On modeling coverage and rate of random cellular networks under generic channel fading," *Wireless Netw.*, vol. 22, no. 8, pp. 2623–2635, Nov. 2016.
- [25] B. Błaszczyszyn, P. Mühlenthaler, and Y. Toor, "Stochastic analysis of aloha in vehicular ad hoc networks," *Ann. Telecommun.*, vol. 68, no. 1-2, pp. 95–106, Jun. 2013.
- [26] B. Błaszczyszyn, P. Mühlenthaler, and Y. Toor, "Maximizing throughput of linear vehicular ad-hoc networks (VANETs)—A stochastic approach," in *Proc. IEEE Eur. Wireless Conf.*, 2009, pp. 32–36.
- [27] Z. Tong, H. Lu, M. Haenggi, and C. Poellabauer, "A stochastic geometry approach to the modeling of DSRC for vehicular safety communication," *IEEE Trans. Intell. Transp. Syst.*, vol. 17, no. 5, pp. 1448–1458, Feb. 2016.
- [28] H.-Y. Tseng, Y.-L. Wei, A.-L. Chen, H.-P. Wu, H. Hsu, and H.-M. Tsai, "Characterizing link asymmetry in vehicle-to-vehicle visible light communications," in *Proc. IEEE Veh. Netw. Conf.*, Dec. 2015, pp. 88–95.
- [29] E. Steinmetz, M. Wildemeersch, T. Q. Quek, and H. Wymeersch, "A stochastic geometry model for vehicular communication near intersections," in *Proc. IEEE Globecom Workshops*, Dec. 2015, pp. 1–6.
- [30] Y. Wang, F. Liu, C. Wang, P. Wang, and Y. Ji, "Stochastic geometric analysis in cooperative vehicular networks under Weibull fading," *IEEE Access*, vol. 7, pp. 158 655–158 670, Oct. 2019.
- [31] N. P. Chandrasekharamenon and B. AncharaV, "Connectivity analysis of one-dimensional vehicular ad hoc networks in fading channels," *EURASIP J. Wireless Commun. and Netw.*, vol. 2012, no. 1, Jan. 2012, pp. 1–16.
- [32] W. Viriyasitavat, S. Yu, and H. Tsai, "Short paper: Channel model for visible light communications using off-the-shelf scooter taillight," in *Proc. IEEE Veh. Netw. Conf.*, Dec. 2013, pp. 170–173.
- [33] Z. Cui, C. Wang, and H. Tsai, "Characterizing channel fading in vehicular visible light communications with video data," in *Proc. IEEE Veh. Netw. Conf.*, Dec. 2014, pp. 226–229.
- [34] L. Zeng *et al.*, "High data rate multiple input multiple output (MIMO) optical wireless communications using white LED lighting," *IEEE J. Sel. Areas Commun.*, vol. 27, no. 9, pp. 1654–1662, Dec. 2009.
- [35] I. S. Gradshteyn and I. M. Ryzhik, *Table of Integrals, Series, and Products*. New York, NY, USA: Academic, 2014.
- [36] A. Goldsmith, *Wireless Communications*. Cambridge, U.K.: Cambridge Univ. Press, 2005.
- [37] Y. Liu, A. Ghazal, C.-X. Wang, X. Ge, Y. Yang, and Y. Zhang, "Channel measurements and models for high-speed train wireless communication systems in tunnel scenarios: A survey," *Sci. China Info. Sci.*, vol. 60, no. 10, Mar. 2017, Art. no. 101301.
- [38] C. Chen, M. Ijaz, D. Tsonev, and H. Haas, "Analysis of downlink transmission in DCO-OFDM-based optical attocell networks," in *Proc. IEEE Global Commun. Conf.*, Feb. 2015, pp. 2072–2077.
- [39] A. Surampudi and R. K. Ganti, "Interference characterization in downlink Li-Fi optical attocell networks," *IEEE J. Lightw. Technol.*, vol. 36, no. 16, pp. 3211–3228, Aug. 2018.
- [40] M. Rahaim and T. D. Little, "Optical interference analysis in visible light communication networks," in *Proc. IEEE Int. Conf. Commun. Workshop*, 2015, pp. 1410–1415.
- [41] N. Ehsan and R. Cruz, "On the optimal SINR in random access networks with spatial reuse," in *Proc. IEEE 40th Annu. Conf. Inf. Sci. Syst.*, Mar. 2006, pp. 938–944.
- [42] J. Gil-Pelaez, "Note on the inversion theorem," *Biometrika*, vol. 38, no. 3/4, pp. 481–482, Dec. 1951.
- [43] J. H. Banks, "Two-capacity phenomenon at freeway bottlenecks: A basis for ramp metering?" *Transp. Res. Rec.*, no. 1320, pp. 83–90, Feb. 1991.
- [44] J. Choi, V. Marojevic, R. Nealy, J. H. Reed, and C. B. Dietrich, "DSRC and IEEE 802.11 ac adjacent channel interference assessment for the 5.9 GHz band," in *Proc. IEEE 89th Veh. Technol. Conf. Spring*, Apr. 2019, pp. 1–5.
- [45] G. Singh, A. Srivastava, and V. A. Bohara, "Impact of weather conditions and interference on the performance of VLC based V2V communication," in *Proc. IEEE 21st Int. Conf. Transparent Opt. Netw.*, 2019, pp. 1–4.
- [46] G. Singh, A. Srivastava, and V. Bohara, "On feasibility of VLC based car-to-car communication under solar irradiance and fog conditions," in *Proc. ACM 1st Int. Workshop Commun. Comput. Connected Veh. Platooning*, Feb. Oct. 2018, pp. 1–7.